

# Consolidation of ultrafine-grained Cu powder and nanostructured Cu–(2.5–10) vol%Al<sub>2</sub>O<sub>3</sub> composite powders by powder compact forging

A. Mukhtar · D. L. Zhang · C. Kong ·  
P. Munroe

Received: 23 February 2010/Accepted: 24 May 2010/Published online: 9 June 2010  
© Springer Science+Business Media, LLC 2010

**Abstract** An as-received ultrafine-grained Cu powder and four nanostructured Cu–(2.5–10) vol%Al<sub>2</sub>O<sub>3</sub> composite powders produced by high-energy mechanical milling of mixtures of the Cu powder and an Al<sub>2</sub>O<sub>3</sub> nanopowder were consolidated using warm powder compaction followed by open die powder compact forging. The circular discs produced in the experiments achieved full densification. Tensile testing of the specimens cut from the forged discs showed that the Cu-forged disc had a fairly high yield strength of 330 MPa, UTS of 340 MPa and a plastic strain to fracture of 15%, but the Cu–Al<sub>2</sub>O<sub>3</sub> composite-forged discs did not show any macroscopic plastic yielding. The fracture strength of the composite-forged discs decreased almost linearly with the increase of the volume fraction of Al<sub>2</sub>O<sub>3</sub> nanoparticles. This study shows that a high level of consolidation of the ultrafine-grained Cu powder and the nanostructured Cu–2.5 vol%Al<sub>2</sub>O<sub>3</sub> composite powder has been achieved by warm powder compacting at 350 °C and powder compact forging at 500 and 700 °C. However, this is not true for the nanostructured Cu–(5, 7.5 and 10) vol%Al<sub>2</sub>O<sub>3</sub> composite powders, possibly due to their higher powder particle hardness at elevated temperatures in the range of 350–800 °C.

## Introduction

Thermomechanical powder consolidation [TPC] processes have been widely used to consolidate nanostructured powders and nanopowders to produce bulk nanostructured and ultrafine-structured metallic materials including metals, alloys and metal matrix composites. The TPC processes involve plastic deformation of the powder particles in a powder compact which can assist rapid densification of the powder compact and establishment of a high level of interparticle atomic bonding through creating new and atomically fresh surfaces and fragmenting old oxide (or hydroxide) surface layers on the powder particles [1, 2]. The TPC processes which have been used include equal channel angular pressing/extrusion (ECAP/ECAE) [3–5], high pressure torsion (HPT) [6–9], powder compact forging (PCF) [2, 10, 11], powder compact extrusion (PCE) [12–14], hot pressing/sinter forge combined with conventional heating [15, 16] or spark plasma heating [17–20] and high-energy mechanical milling (HEMM) [21–24]. Although TPC processes have been used widely to synthesize bulk nanostructured or ultrafine structured metallic materials for mechanical testing and microstructural characterisation, systematic studies on the TPC processes themselves are still lacking. For this reason, our group has paid close attention to the actual process of consolidation, instead of just focusing on studying the microstructure and mechanical properties of the synthesized materials. In this study, we utilised one of the TPC processes, PCF, to consolidate an as-received ultrafine-grained Cu powder that was produced using an electrolytic process and four nanostructured Al–(2.5–10) vol%Al<sub>2</sub>O<sub>3</sub> composite powders that were produced in-house by using HEMM, and investigated the mechanical and fracture behaviour of the forged discs. The objective of the study is to establish the

A. Mukhtar · D. L. Zhang (✉)  
Waikato Centre for Advanced Materials (WaiCAM),  
Department of Engineering, The University of Waikato,  
Hamilton, New Zealand  
e-mail: d.zhang@waikato.ac.nz

C. Kong · P. Munroe  
Electron Microscope Unit, The University of New South Wales,  
Sydney, Australia

possible links between the nature of the powders and the consolidation state of the bulk samples as reflected by the level of densification and interparticle bonding.

## Experimental procedure

The nanostructured Cu–Al<sub>2</sub>O<sub>3</sub> composite powders with four nominal compositions: Cu–2.5 vol%Al<sub>2</sub>O<sub>3</sub>, Cu–5 vol%Al<sub>2</sub>O<sub>3</sub>, Cu–7.5 vol%Al<sub>2</sub>O<sub>3</sub> and Cu–10 vol%Al<sub>2</sub>O<sub>3</sub> were prepared using HEMM of a mixture of Cu powder (99.7% pure, particle size: 1–63 µm) and Al<sub>2</sub>O<sub>3</sub> nanopowder (99.9% pure, average particle size: 50 nm) under an inert atmosphere of argon. The HEMM process consisted of two steps of 12 h long each, and the details of the powder milling process have been reported in Ref. [25]. As-received pure Cu powder and mechanically milled nanostructured Cu–(2.5–10) vol%Al<sub>2</sub>O<sub>3</sub> composite powders were first compacted by uniaxial hot pressing at 350 °C for 20 min under a pressure of 300 MPa with a cylindrical H13 steel die set (with an internal diameter of 25 mm) and a hydraulic press. For the powder compact forging experiments, the Cu and Cu–Al<sub>2</sub>O<sub>3</sub> composite powder compacts were heated from room temperature to designated temperatures in the range of 500–800 °C using induction heating under an inert atmosphere of argon with the oxygen content being controlled to be less than 200 ppm. Once a powder compact was heated to the designated temperature, it was held at the temperature for a very short time of no more than 5 s, and then taken from the induction heating coil to be placed on the top of the lower half of an open die set kept at room temperature. Once the heated powder compact was in place, the upper half of the open die set was brought down at a speed of 7 mm/s using a 100-ton hydraulic press to upset forge the cylindrical powder compact into a circular disc. The thickness of the discs was controlled by the balance between the force of the press and the resistance of the sample which rapidly increased with increasing area and decreasing temperature, and was in the range of 6.2–8.2 mm. Flat dog-bone-shaped tensile testing specimens were cut from the forged discs using an electric discharge machining (EDM) wire cutter. The tensile test specimens had dimensions of approximately 9 × 2 × 2 mm<sup>3</sup> within their gauge lengths. The tensile testing was performed at room temperature using an Instron 4204 testing machine with a strain rate of  $6 \times 10^{-5}$  s<sup>-1</sup>. In tensile testing, the specimen was gripped using holders which held the two heads of the specimen by matching the female shape of the holder with the male shape of the head of the specimen. The characterization of the powders, consolidated samples and fractured tensile testing specimens were performed using a number of standard material

characterisation techniques. They include X-ray diffractometry (XRD) (Philips X-pert X-ray diffraction system, Cu K $\alpha$  radiation and a graphite monochromator), scanning electron microscopy (SEM)(Hitachi S4000 SEM), transmission electron microscopy (TEM) and scanning transmission electron microscopy (STEM) (both using a Philips/FEI CM200 TEM) and Vickers microhardness testing with a load of 25 g and a loading duration of 20 s. A dual beam focused ion beam microscope was used to produce the TEM specimens from powder particles and selected consolidated samples.

## Results

### Powder characterisation

As shown by the SEM images in Fig. 1, the as-received Cu powder particles had snow flake-like shapes with dendrite branches due to the fact that they were produced by electrolytic reduction, while the as-milled Cu–Al<sub>2</sub>O<sub>3</sub> composite powder particles had irregular and equiaxed shapes. The sizes of the powder particles were in the ranges of 10–100 µm for the Cu powder, 20–100 µm for the Cu–(2.5 and 5) vol%Al<sub>2</sub>O<sub>3</sub> composite powders and 10–50 µm for Cu–(7.5 and 10) vol%Al<sub>2</sub>O<sub>3</sub> composite powders. Figure 2 shows the XRD patterns of the as-received Cu and as-milled Cu–Al<sub>2</sub>O<sub>3</sub> composite powders. Using the XRD patterns and the Williamson–Hall method [26], the average grain size and lattice strain of the powder particles were estimated, and the results are shown in Fig. 3. The lattice strain of the powder particles is mainly caused by the dislocations in the grains of the powder particles, and it is proportional to the dislocation density. The average grain size of the as-received Cu powder particles was estimated to be 277 nm, while those of the as-milled the Cu–(2.5, 5, 7.5 and 10) vol%Al<sub>2</sub>O<sub>3</sub> composite powder particles were estimated to be 62, 54, 28, and 100 nm respectively. The lattice strain of the as-received Cu powder particles was estimated to be 0.31%, while those of the as-milled composite powder particles were clearly higher, being in the range of 0.51–1.32%, suggesting that the dislocation density in the as-milled composite particles was high. The ultrafine-grained structure of the as-received Cu powder particles and the nanostructure of the as-milled Cu–Al<sub>2</sub>O<sub>3</sub> composite powder particles were also confirmed by TEM examination. As shown in Figs. 4 and 5, the grains of the as-received Cu powder particles had sizes in the range of 0.2–0.6 µm, while the grains of the Cu matrix of the as-milled Cu–Al<sub>2</sub>O<sub>3</sub> composite powder particles had sizes in the range of 20–100 nm. The XRD patterns of the Cu–Al<sub>2</sub>O<sub>3</sub> composite powders did not show any Al<sub>2</sub>O<sub>3</sub> peaks, even for the Cu–10 vol%Al<sub>2</sub>O<sub>3</sub> composite. This is

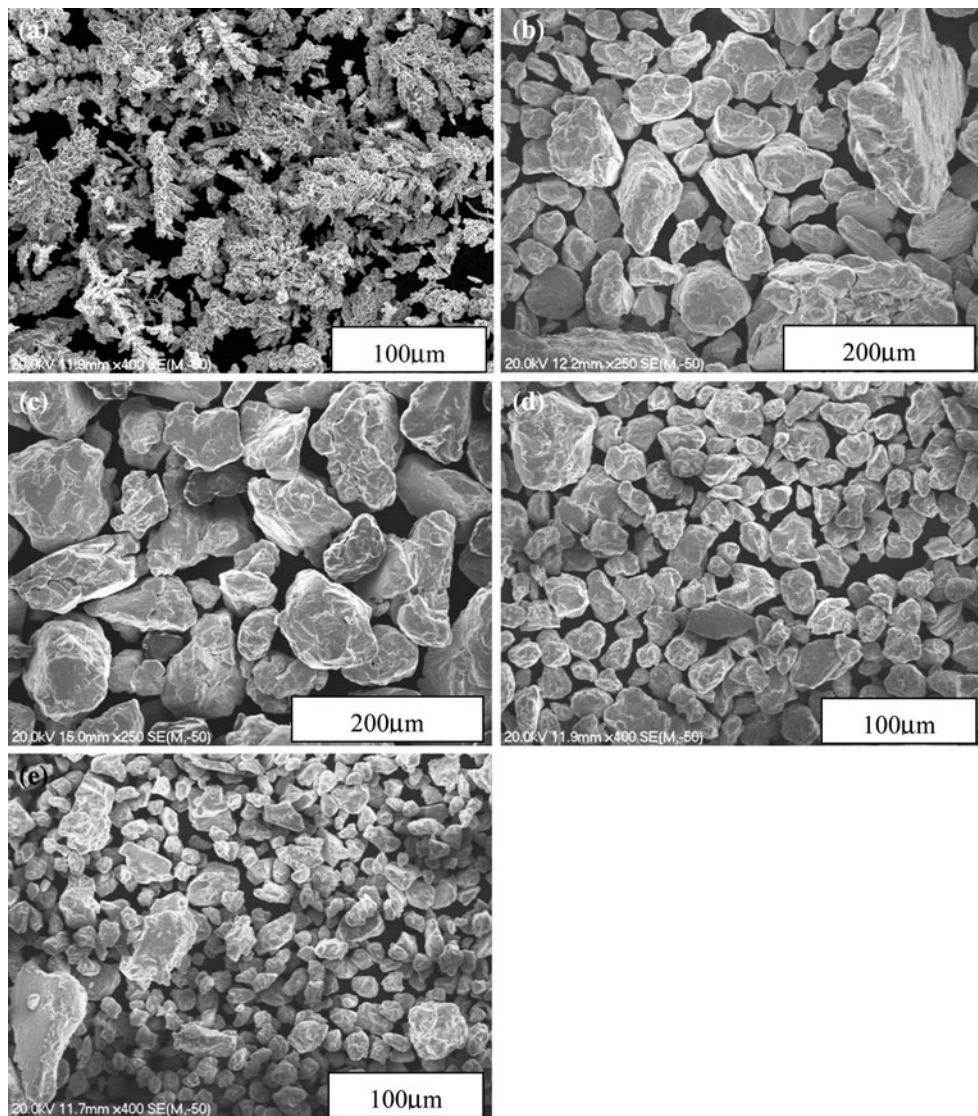


**Fig. 1** SEM micrographs of as-received Cu powder particles and Cu–Al<sub>2</sub>O<sub>3</sub> composite powder particles produced by HEMM: **a** Cu; **b** Cu–2.5 vol% Al<sub>2</sub>O<sub>3</sub>; **c** Cu–5 vol% Al<sub>2</sub>O<sub>3</sub>; **d** Cu–7.5 vol% Al<sub>2</sub>O<sub>3</sub>; and **e** Cu–10 vol% Al<sub>2</sub>O<sub>3</sub>

likely due to the relatively small fractions of Al<sub>2</sub>O<sub>3</sub> nanoparticles in the composite powders, and the low level of crystallinity of Al<sub>2</sub>O<sub>3</sub> nanoparticles. The TEM bright field images of the Cu–Al<sub>2</sub>O<sub>3</sub> composite powder particles showed some contrast of the Al<sub>2</sub>O<sub>3</sub> particles.

Scanning transmission electron microscopy (STEM) imaging and EDX X-ray Cu and Al elemental mappings of the as-milled Cu–Al<sub>2</sub>O<sub>3</sub> powder particles (Fig. 6) confirmed that the Al<sub>2</sub>O<sub>3</sub> nanoparticles were embedded in the Cu matrix, and in the meantime, also showed that part of the Al<sub>2</sub>O<sub>3</sub> nanoparticles were dissolved in the Cu matrix as a result of milling. With increasing the volume fraction of the Al<sub>2</sub>O<sub>3</sub> from 2.5 to 10 vol%, the diffraction angle of the Cu{111} peak gradually decreased by up to 0.08°, and this corresponded to an increase of the Cu lattice parameter by up to 0.0013 nm. This Cu lattice

parameter increase of the mechanically milled Cu–Al<sub>2</sub>O<sub>3</sub> composite powders is likely to be due to non-equilibrium dissolution of Al<sub>2</sub>O<sub>3</sub> nanoparticles into the Cu matrix causing an increase of the Al<sup>3+</sup> concentration in the Cu lattice during milling. The result of the XRD analysis was in agreement with that of X-ray mappings in showing that some Al<sub>2</sub>O<sub>3</sub> nanoparticles were dissolved into the Cu matrix during HEMM.

The values of the average microhardness of the as-received Cu powder particles and as-milled Cu–Al<sub>2</sub>O<sub>3</sub> composite powder particles are shown in Fig. 7. As expected, the average microhardness of the Cu powder particles was fairly low, being 0.98 GPa, while that of the as-milled Cu–(2.5, 5, 7.5 and 10) vol% Al<sub>2</sub>O<sub>3</sub> composite powder particles was much higher, being 2.52, 2.63, 2.60 and 2.50 GPa, respectively.

**Fig. 2** XRD patterns of as-received Cu powder and Cu–Al<sub>2</sub>O<sub>3</sub> composite powders produced by HEMM: (a) Cu; (b) Cu–2.5 vol% Al<sub>2</sub>O<sub>3</sub>; (c) Cu–5 vol% Al<sub>2</sub>O<sub>3</sub>; (d) Cu–7.5 vol% Al<sub>2</sub>O<sub>3</sub>; and (e) Cu–10 vol% Al<sub>2</sub>O<sub>3</sub> (the dashed line is used to reflect the amount of Cu{111} peak shift with increasing Al<sub>2</sub>O<sub>3</sub> volume fraction)

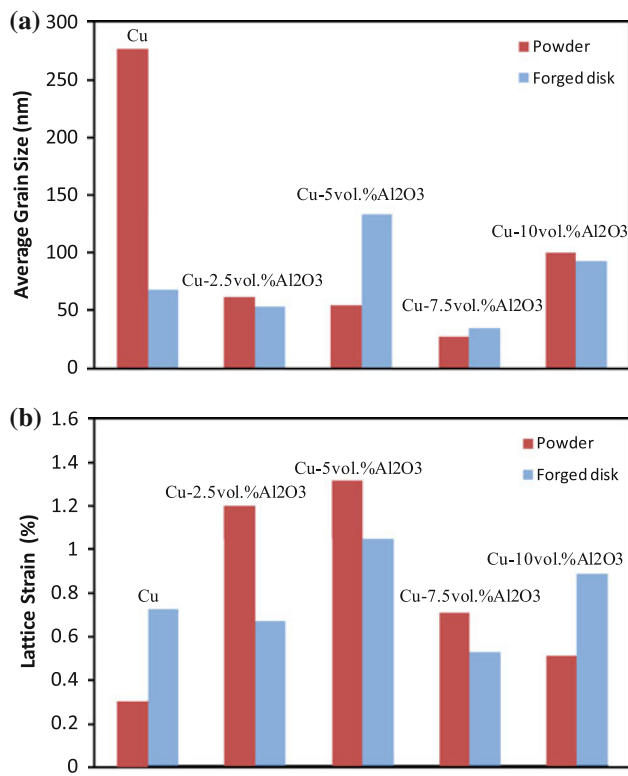
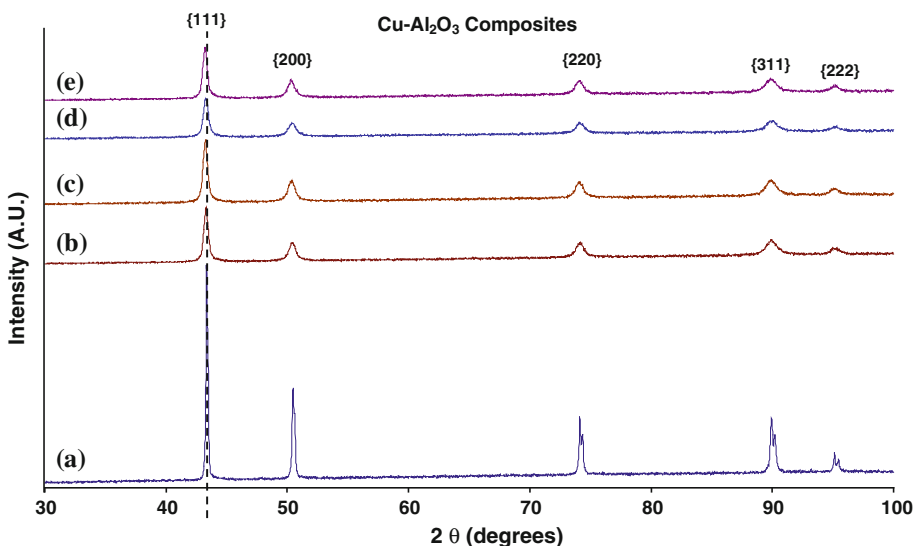


**Fig. 3** The average grain size and lattice strain of as-received Cu powder particles and as-milled Cu–Al<sub>2</sub>O<sub>3</sub> composite powder particles and those of corresponding forged discs, respectively: **a** average grain size; and **b** lattice strain

#### Powder consolidation

As shown in Table 1, the cylindrical Cu and Cu–Al<sub>2</sub>O<sub>3</sub> composite powder compacts produced after warm pressing had a diameter of 25 mm and a height in the range of 18–28 mm. Table 1 also shows the theoretical density of

Cu and Cu–Al<sub>2</sub>O<sub>3</sub> composites and the measured absolute and relative densities of the Cu and Cu–Al<sub>2</sub>O<sub>3</sub> composite powder compacts. The theoretical density of the Cu–Al<sub>2</sub>O<sub>3</sub> composites was calculated using the rule of mixture, while the actual densities of the Cu and Cu–Al<sub>2</sub>O<sub>3</sub> composite powder compacts were measured by dividing their weights with their volumes. As shown in Table 1, a high relative density of the Cu powder compact (97%) was achieved by warm pressing. With the same warm pressing condition, the relative density achieved with the Cu–2.5 vol% Al<sub>2</sub>O<sub>3</sub> powder compact was considerably lower, being 88%. With increase of the Al<sub>2</sub>O<sub>3</sub> volume fraction to 5 vol%, the relative density of the Cu–Al<sub>2</sub>O<sub>3</sub> composite powder compact decreased further to 76%. For some reason, the relative density of the Cu–Al<sub>2</sub>O<sub>3</sub> powder compact increased slightly to 80% with further increase of the Al<sub>2</sub>O<sub>3</sub> volume fraction to 10 vol%.

The temperature versus time curves of the Cu and Cu–Al<sub>2</sub>O<sub>3</sub> composite powder compacts during induction heating were almost linear, and from them, the average heating rate of each of the powder compacts was determined. The temperatures to which the powder compacts were heated to prior to forging and the corresponding average heating rates are given in Table 2, and it can be seen that the average heating rates achieved by induction heating of the Cu and Cu–Al<sub>2</sub>O<sub>3</sub> composite powder compacts were very high, being in the range of 300–650 °C/min. The discs produced by the open die powder compact forging had a thickness in the range of 6.2–8.2 mm, as shown in Table 2, and this corresponded to a height reduction in the range of 65–75%. All the forged discs had cracks at their peripheral edges (Fig. 8) which were likely caused by the tensile stress in stretching the material along the peripheral direction and low tensile strength of the powder compact in the process of consolidation.

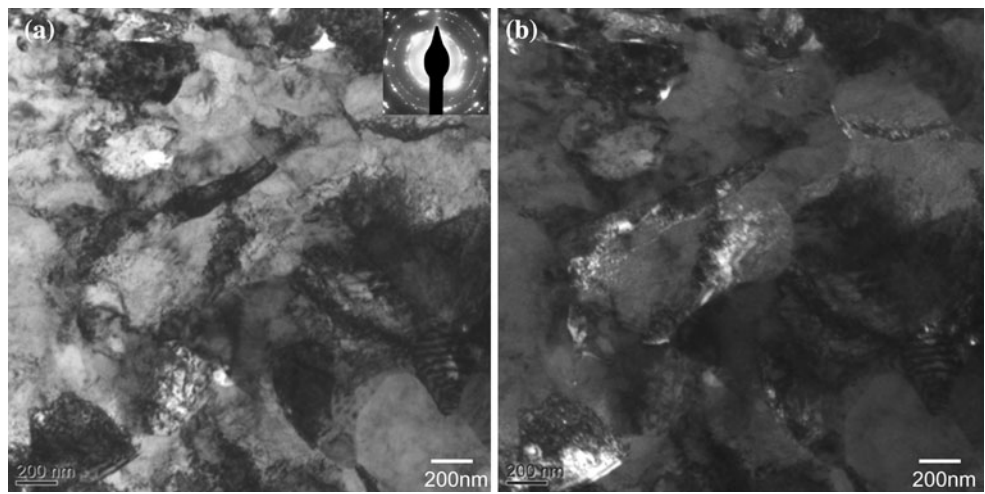


**Fig. 4** TEM bright field and corresponding dark field images (**a** and **b**) and SADP (*inset*) of an as-received Cu powder particle

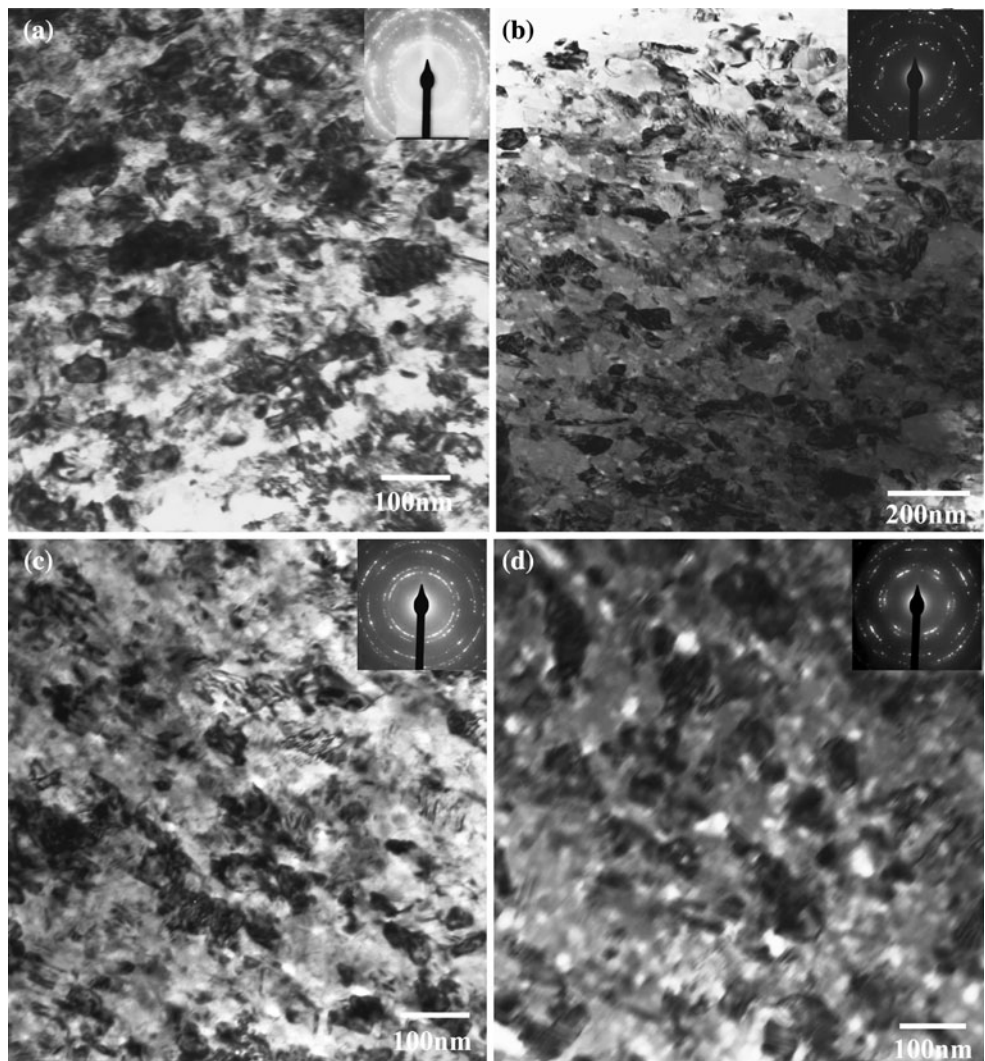


**Fig. 5** TEM bright field images and SADPs (*inset*) of Cu–Al<sub>2</sub>O<sub>3</sub> composite powder particles produced by HEMM: **a** Cu–2.5 vol%Al<sub>2</sub>O<sub>3</sub>; **b** Cu–5 vol%Al<sub>2</sub>O<sub>3</sub>; **c** Cu–7.5 vol%Al<sub>2</sub>O<sub>3</sub>; and **d** Cu–10 vol%Al<sub>2</sub>O<sub>3</sub>

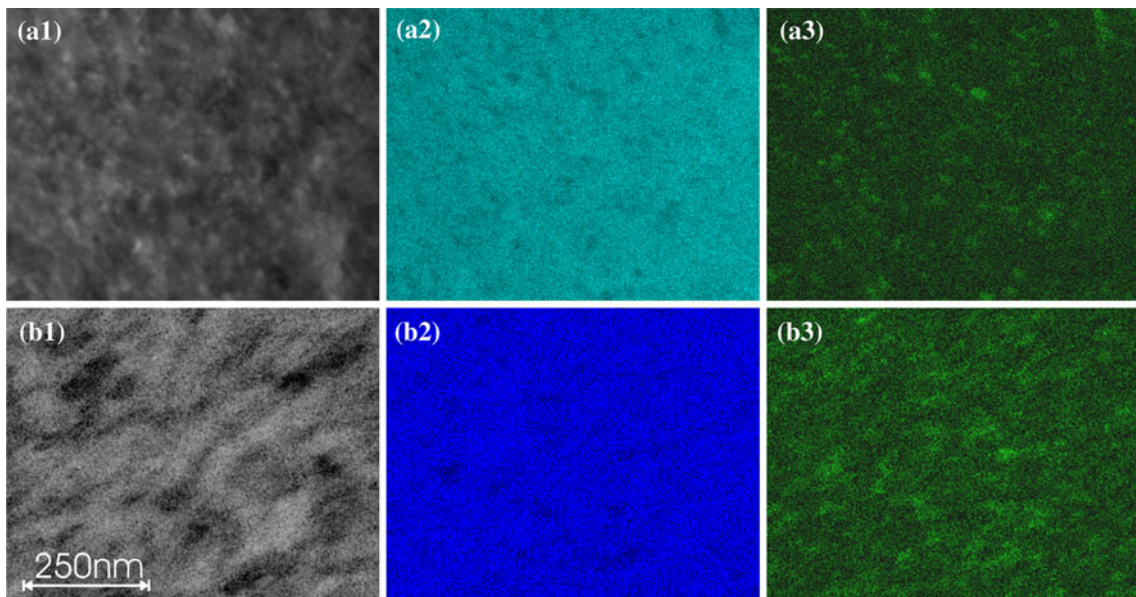


**Fig. 6** STEM images (**a1** and **b1**) and EDX mappings of Cu (**a2** and **b2**) and Al (**a3** and **a4**) elements of as milled Cu–2.5 vol%Al<sub>2</sub>O<sub>3</sub> composite powder (**a1**, **a2** and **a3**) and Cu–10 vol%Al<sub>2</sub>O<sub>3</sub> composite powder (**b1**, **b2** and **b3**), respectively

**Fig. 7** The average microhardness of as-received Cu powder particles and as-milled Cu–Al<sub>2</sub>O<sub>3</sub> composites powder particles and corresponding forged discs

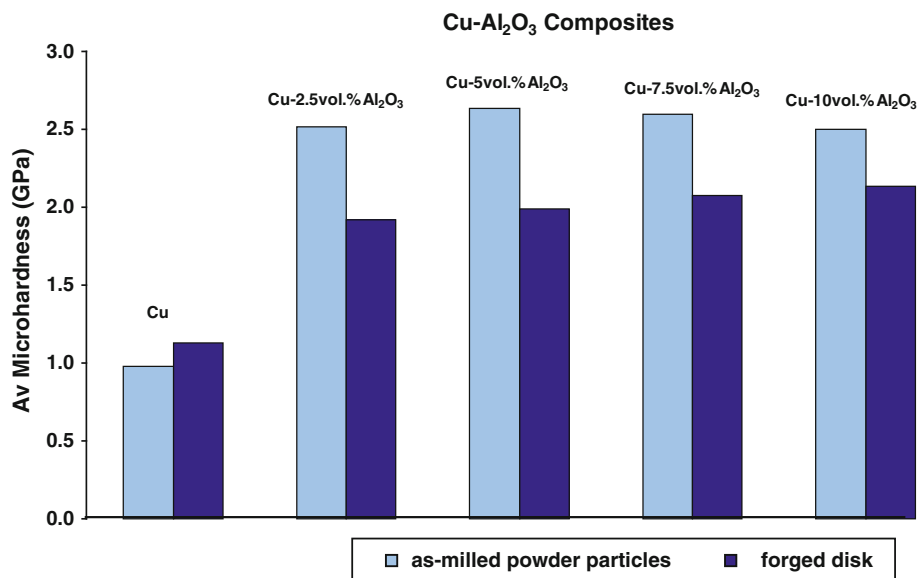


**Table 1** The theoretical density of Cu and Cu–Al<sub>2</sub>O<sub>3</sub> composites, the measured density, relative density and height of Cu and Cu–Al<sub>2</sub>O<sub>3</sub> composite powder compacts

Material	Theoretical density (g/cm <sup>3</sup> )	Measured density (g/cm <sup>3</sup> )	Relative density (%)	Compact height (mm)
Cu	8.93	8.78	97	18.1
Cu–2.5 vol%Al <sub>2</sub> O <sub>3</sub>	8.81	7.84	88	20.7
Cu–5 vol%Al <sub>2</sub> O <sub>3</sub>	8.68	6.61	76	26.4
Cu–7.5 vol%Al <sub>2</sub> O <sub>3</sub>	8.56	6.68	78	25.6
Cu–10 vol%Al <sub>2</sub> O <sub>3</sub>	8.44	6.77	80	27.7

The SEM examination of the Cu and Cu–Al<sub>2</sub>O<sub>3</sub> composite-forged discs showed that there were no pores in the discs, suggesting that the forged discs were fully dense.

As shown in Fig. 9, the Cu peaks in the XRD patterns of the Cu and Cu–Al<sub>2</sub>O<sub>3</sub> composite-forged discs all exhibited clear broadening. Again, using the XRD patterns and the

**Table 2** The temperatures and average heating rates of the Cu and Cu-Al<sub>2</sub>O<sub>3</sub> composite powder compacts and the thickness and height reduction of the Cu and Cu-Al<sub>2</sub>O<sub>3</sub> composite-forged discs

Material	Compact temperature (°C)	Avg. heating rate (°C/min)	Forged disc thickness (mm)	Height reduction during forging (%)
Cu	500	300	6.2	66
Cu-2.5 vol%Al <sub>2</sub> O <sub>3</sub>	700	350	8.2	60
Cu-5 vol%Al <sub>2</sub> O <sub>3</sub>	700	650	6.8	74
Cu-7.5 vol%Al <sub>2</sub> O <sub>3</sub>	700	500	6.5	75
Cu-10 vol%Al <sub>2</sub> O <sub>3</sub>	800	450	7.2	74

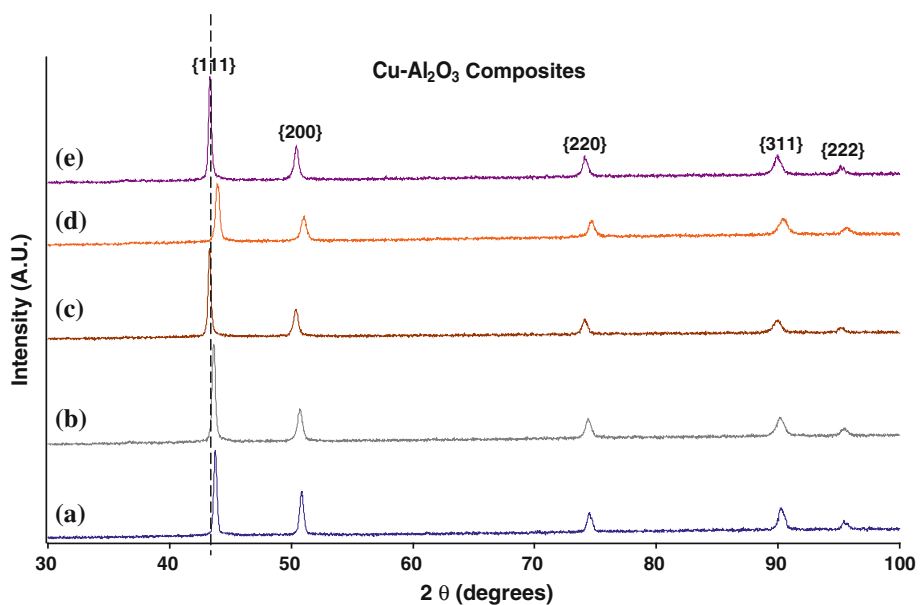


**Fig. 8** The Cu disc produced by powder compact forging (the image also shows the location and shape of the tensile testing specimens cut from the forged disc)

Williamson–Hall method [26], the average grain sizes and lattice strains of the forged discs were estimated, and the results are also shown in Fig. 3. The average grain size of the Cu-forged disc was estimated to be 68 nm, which is dramatically smaller than that of the as-received Cu powder particles. The nanocrystalline structure of the Cu disc was confirmed by TEM examination (Fig. 10) which showed that the grain sizes were in the range of

50–200 nm. The average grain sizes of the Cu matrix in the Cu-(2.5, 7.5 and 10) vol%Al<sub>2</sub>O<sub>3</sub> composite-forged discs were estimated to be 53, 35 and 93 nm, all being very close to those of the corresponding as-milled composite powder particles. However, the average grain size of the Cu matrix in the Cu-5 vol%Al<sub>2</sub>O<sub>3</sub>-forged disc was dramatically higher than that of the corresponding as-milled composite powder particles, being 133 nm. Further investigation is needed to clarify the reasons for this significant grain coarsening. Based on the results of the Williamson–Hall analysis, the lattice strains of the Cu and Cu-10 vol%Al<sub>2</sub>O<sub>3</sub>-forged discs were higher than those of the corresponding powder particles, while that of the Cu-(2.5, 5 and 7.5) vol%Al<sub>2</sub>O<sub>3</sub> composite-forged discs were lower than those of corresponding powder particles. The Cu peaks in the XRD patterns of the Cu and Cu-Al<sub>2</sub>O<sub>3</sub> composite-forged discs all shifted to higher angles than those of the corresponding as-received Cu powder and as-milled Cu-Al<sub>2</sub>O<sub>3</sub> composite powders. For Cu, this is likely due to oxygen pick up during the consolidation process. For Cu-Al<sub>2</sub>O<sub>3</sub> composites, it was observed that the Cu peaks in the XRD patterns of the Cu-(5 and 10) vol%Al<sub>2</sub>O<sub>3</sub> composite-forged discs shifted to the positions which are almost the same as those of pure Cu.

**Fig. 9** X-ray diffraction patterns of Cu and Cu-Al<sub>2</sub>O<sub>3</sub> composite-forged discs: (a) Cu; (b) Cu-2.5 vol%Al<sub>2</sub>O<sub>3</sub>; (c) Cu-5 vol%Al<sub>2</sub>O<sub>3</sub>; (d) Cu-7.5 vol%Al<sub>2</sub>O<sub>3</sub>; and (e) Cu-10 vol%Al<sub>2</sub>O<sub>3</sub> (the dash line indicates the position of {111} peak of pure Cu)



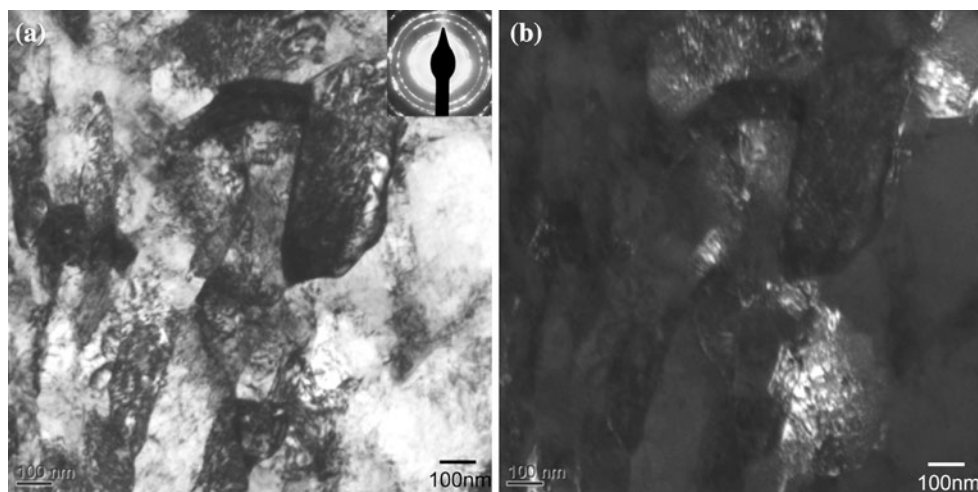


**Fig. 10** TEM bright field and corresponding dark field images (**a** and **b**) and SADP (*inset*) of the Cu disc produced by powder compact forging

This shows that the  $\text{Al}_2\text{O}_3$  dissolved into the Cu matrix during milling precipitated out during consolidation. On the other hand, the Cu peaks in the XRD pattern of the Cu–(2.5 and 7.5) vol% $\text{Al}_2\text{O}_3$  composite-forged discs shifted more significantly to angles which were clearly higher than those of pure Cu. This may be partly due to the precipitation of the dissolved  $\text{Al}_2\text{O}_3$  and partly due to oxygen pick-up during powder consolidation.

#### Mechanical behaviour of the forged discs

As shown in Fig. 7, the average microhardness values of the Cu and Cu–(2.5, 5, 7.5 and 10) vol% $\text{Al}_2\text{O}_3$  composite-forged discs were 1.13, 1.92, 1.99, 2.08 and 2.14 GPa respectively. Figure 11 shows the typical tensile engineering stress–engineering strain curves of the specimens cut from the Cu and Cu– $\text{Al}_2\text{O}_3$  composite-forged discs, as shown in Fig. 8. The tensile testing showed that the Cu-forged disc had a yield strength, ultimate tensile strength (UTS) and plastic strain to fracture of 330 MPa, 340 MPa and 15%, respectively (Fig. 11). However, as shown in Fig. 11, the Cu– $\text{Al}_2\text{O}_3$  composite-forged discs did not show any macroscopic plastic yielding, and the fracture strength of forged discs decreased almost linearly from 660 to 130 MPa with the increase of the volume fraction of  $\text{Al}_2\text{O}_3$  nanoparticles from 2.5 to 10 vol%. It should be noted that the slope of the elastic part of the stress–strain curves is quite low in comparison with the expected Young’s modulus of the materials. This discrepancy is caused by the small slip of the specimens in the grips during loading. However, this discrepancy would not affect the measurement of the plastic strain because the slip would stop once the material starts yielding because the load stops increasing. This discrepancy can be prevented if an extensometer is used to measure the strain.

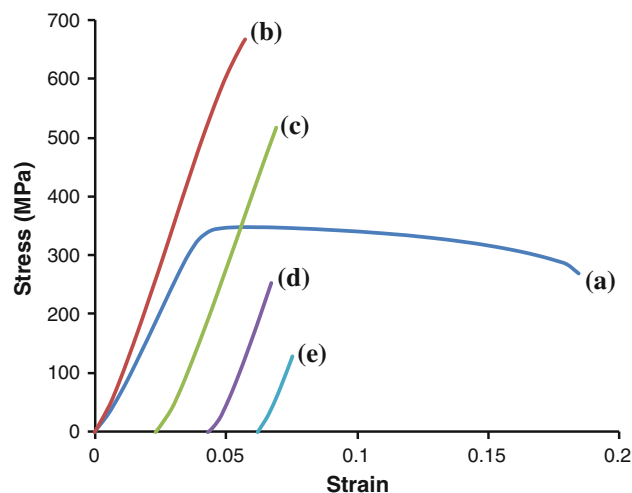


**Fig. 11** Tensile stress–strain curves of the specimens cut from the Cu and Cu– $\text{Al}_2\text{O}_3$  composite-forged discs: (a) Cu; (b) Cu–2.5 vol% $\text{Al}_2\text{O}_3$ ; (c) Cu–5 vol% $\text{Al}_2\text{O}_3$ ; (d) Cu–7.5 vol% $\text{Al}_2\text{O}_3$ ; and (e) Cu–10 vol% $\text{Al}_2\text{O}_3$  (curves (c), (d) and (e) are shifted to the right from the origin of the coordinate for clarity)

Unfortunately, this cannot be done in this study due to the small specimen size.

The broken tensile testing specimens cut from the Cu-forged disc exhibited clear necking prior to fracturing, as shown in Fig. 12a. The necking of the tensile testing specimens observed was in agreement with the shape of the tensile stress–strain curves of the Cu-forged disc (Fig. 11) which showed that the engineering stress reached the peak value at a fairly small plastic strain. On the other hand, the broken tensile testing specimens cut from the Cu– $\text{Al}_2\text{O}_3$  composite-forged discs did not show any necking, as shown in Fig. 12b–d. It was also observed (Fig. 12) that the Cu and Cu–2.5 vol% $\text{Al}_2\text{O}_3$  composite tensile testing specimens fractured at locations near the middle of the

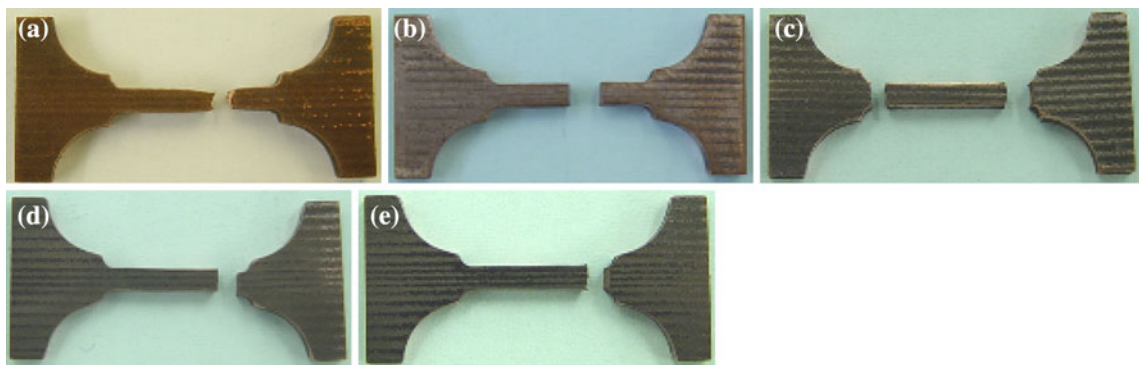


**Fig. 12** Broken tensile test specimens from the Cu and Cu–Al<sub>2</sub>O<sub>3</sub> composite-forged discs: **a** Cu; **b** Cu–2.5 vol%Al<sub>2</sub>O<sub>3</sub>; **c** Cu–5 vol%Al<sub>2</sub>O<sub>3</sub>; **d** Cu–7.5 vol%Al<sub>2</sub>O<sub>3</sub>; and **e** Cu–10 vol%Al<sub>2</sub>O<sub>3</sub>

gauge length, while the Cu–(5, 7.5 and 10) vol%Al<sub>2</sub>O<sub>3</sub> composite tensile testing specimens fractured at locations close to the locations of section width change.

As shown in Fig. 12, the tensile testing specimens cut from the Cu-forged disc showed a cup-and-cone fracture surface morphology, while those cut from the Cu–Al<sub>2</sub>O<sub>3</sub> composite-forged discs showed flat tensile fracture surface morphology. SEM examination of the fracture surfaces of the broken tensile testing specimens showed that the Cu-forged disc exhibited typical ductile fracture with micrometer-sized dimples covering the whole area of the fracture surface, as shown in Fig. 13a. The fracture surface of the Cu–2.5 vol%Al<sub>2</sub>O<sub>3</sub>-forged disc also showed micrometer-sized dimples that reflect ductile fracture, but it appeared that the dimples did not cover the whole fracture surface, as shown in Fig. 13b. The part of the fracture surface which was not covered by dimples showed a feature which indicated particle debonding. The fracture surfaces of the Cu–(5, 7.5 and 10) vol% (Fig. 13c–e) did not show any regions with clear dimples, and more clearly indicated that the specimens fractured predominantly through particle debonding.

## Discussion

In this study, several major observations which are important to the study of consolidation of the ultrafine-grained Cu and nanostructured Cu–Al<sub>2</sub>O<sub>3</sub> composite powders have been made. The first observation is that with the same warm pressing temperature and pressure, the density of the Cu powder compact is significantly greater than that of the Cu–2.5 vol%Al<sub>2</sub>O<sub>3</sub> powder compact which is also significantly greater than those of the Cu–(5, 7.5 and 10) vol%Al<sub>2</sub>O<sub>3</sub> powder compacts. It is apparent that the difference between the relative density of the Cu powder compact and those of the Cu–Al<sub>2</sub>O<sub>3</sub> powder compacts is due to the drastic difference between the hardness of the

as-received ultrafine-grained Cu powder particles and that of the as-milled and work-hardened Cu–Al<sub>2</sub>O<sub>3</sub> powder particles. However, the clear difference between the relative density of the Cu–2.5 vol%Al<sub>2</sub>O<sub>3</sub> and those of the other three Cu–Al<sub>2</sub>O<sub>3</sub> powder compacts cannot be attributed to the difference in the powder particle hardness difference, since the particle hardness difference is very small. The possible explanation for the difference in the relative densities of the Cu–Al<sub>2</sub>O<sub>3</sub> powder compacts is that the level of the powder particle softening that occurred during warm pressing at 350 °C is much higher for Cu–2.5 vol%Al<sub>2</sub>O<sub>3</sub> than that for the other Cu–Al<sub>2</sub>O<sub>3</sub> composites due to the increased thermal stability of microstructure of the powder particles with increasing fraction of Al<sub>2</sub>O<sub>3</sub>.

The second observation is that the disc produced by powder compact forging of the ultrafine-grained Cu powder has a much finer microstructure than that of the as-received Cu powder particles as shown by the XRD peak broadening, average grain size estimation using the Williamson–Hall method and TEM examination of as-received Cu powder particles and the Cu-forged disc. This is rather surprising and important, because it shows that the microstructure of Cu is significantly refined rather than coarsened during the consolidation process. Similar grain refinement in consolidation of a microcrystalline Cu powder by ECAE was also observed by Hoauouai et al. [3]. This grain refinement is likely due to recrystallisation of the heavily and plastically deformed ultrafine-grained Cu powder particles in the powder compact during heating to 500 °C. The very high relative density of the Cu powder compact (97%) achieved by warm pressing the Cu powder shows that the amount of plastic deformation of the Cu powder particles in the powder compact is very high, so the likelihood for the recrystallisation to occur in heating the powder compact to 500 °C can be high. Since the powder compact was immediately forged once it reached 500 °C, and the open die forging caused rapid cooling of the powder compact to a temperature below 100 °C, it can

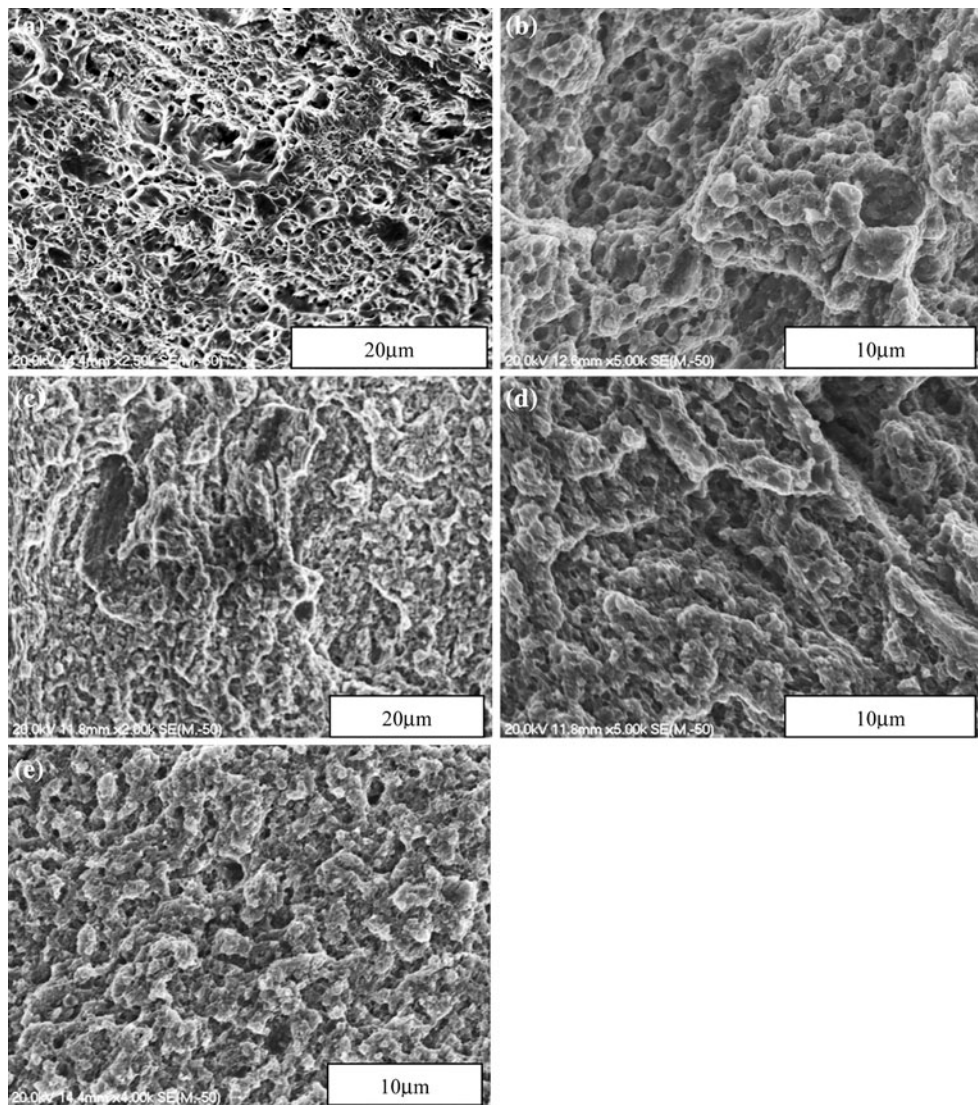


**Fig. 13** SEM micrographs showing the fracture surfaces of the tensile testing specimens cut from the Cu and Cu-Al<sub>2</sub>O<sub>3</sub> composite-forged discs: **a** Cu; **b** Cu-2.5 vol%Al<sub>2</sub>O<sub>3</sub>; **c** Cu-5 vol%Al<sub>2</sub>O<sub>3</sub>; **e** Cu-7.5 vol%Al<sub>2</sub>O<sub>3</sub>; and **d** Cu-10 vol%Al<sub>2</sub>O<sub>3</sub>

be expected that the nanometer-sized grains formed through recrystallisation are mostly kept in the bulk sample.

The third observation is that the Cu grains in Cu-(2.5, 7.5 and 10) vol%Al<sub>2</sub>O<sub>3</sub> powder particles either only become slightly coarsened or become slightly finer in the process of consolidation, and that the Cu-Al<sub>2</sub>O<sub>3</sub>-forged discs have a high hardness in the range of 1.9–2.14 GPa, which is 20–25% lower than that of corresponding powder particles. This is rather surprising since the powder compacts were heated to 700 or 800 °C (for Cu-10 vol%Al<sub>2</sub>O<sub>3</sub> only) which was a fairly high temperature relative to the melting point of Cu ( $0.72T_m$  and  $0.79T_m$ , respectively, where  $T_m$  is the melting point of Cu in Kelvin scale). This shows that the thermal stability of the nanocrystalline structure of the Cu matrix of the Cu-Al<sub>2</sub>O<sub>3</sub> composite is

very high. This is in agreement with the observation made in studying the microhardness and microstructural changes of Cu-10 vol%Al<sub>2</sub>O<sub>3</sub> composite powder particles when annealing for 1 h at different temperatures up to 500 °C [27]. Related to this observation, it has also been found that the average grain sizes of the as-milled Cu-(2.5–10) vol%Al<sub>2</sub>O<sub>3</sub> composite powder particles and those of the corresponding consolidated samples do not show any systematic changes with the volume fraction of Al<sub>2</sub>O<sub>3</sub> nanoparticles (Fig. 3). The lack of correlation between the Al<sub>2</sub>O<sub>3</sub> nanoparticle content and the average grain sizes of the as-milled powder particles may be due to the complexity of the interactions between the composition, size, morphology, microstructure and microhardness of the powder particles, and the dynamics of impacts caused by collisions among the milling balls and between the milling

balls and the container wall. In general, the  $\text{Al}_2\text{O}_3$  nanoparticles in the consolidated samples do show their effectiveness in limiting the growth of Cu grains in the composite powder particles during powder consolidation, but it appears that the magnitude of this effectiveness is independent of the volume fraction of  $\text{Al}_2\text{O}_3$  nanoparticles ranging 2.5–10%. A possible reason for this might be that the time–temperature window of the powder compact forging process used to consolidate the powders in this study is too narrow to allow the change of the effectiveness with changing the volume fractions of  $\text{Al}_2\text{O}_3$  nanoparticles to be shown.

The fourth and most important observation is about the mechanical behaviour of the consolidated samples. For the ultrafine-grained Cu powder, a high level of consolidation close to 100% is achieved even though the powder compact temperature before forging is only 500 °C, which is  $0.57T_m$ . This high level of consolidation is reflected by the fairly high tensile yield strength and UTS and a substantial amount of plastic strain to fracture, and a fracture surface that shows typical ductile fracture and lack of any features indicating the occurrence of particle debonding. Similarly, it can be stated that the level of consolidation of the Cu–2.5 vol% $\text{Al}_2\text{O}_3$  powder is also very high, as reflected by the high fracture strength of the forged disc and the ductile fracture surface (Fig. 13b). However, the forged disc still lacks macroscopic yielding, and this shows that the level of consolidation is still clearly lower than 100%. The SEM examination of the cross section of the forged disc shows it has no pores, so the lack of macroscopic yielding of the material must be caused by particle debonding that occurs at the high stress prior to macroscopic yielding. It can be envisaged that at a high stress of 660 MPa, formation of pores occupying only a few percentage of the volume of the specimen caused by the particle debonding can prevent macroscopic yielding of the material due to the rapid formation and growth of cracks through linking these pores which might be closely spaced. It should be pointed out that the SEM examination of the fracture surface shows that the nanostructured consolidated Cu–2.5 vol% $\text{Al}_2\text{O}_3$  composite material does have a substantial level of intrinsic ductility, and the lack of measured macroscopic ductility is purely due to the particle debonding and thus does not reflect the true nature of the material.

The tensile testing and fracture surface examination of the other three forged discs show clearly that the level of consolidation of the Cu–(5, 7.5 and 10) vol% $\text{Al}_2\text{O}_3$  composite powders is fairly low. The fact that the fracture strength of the consolidated material is much lower than the expected tensile strength of around 700 MPa from the microhardness value and that the consolidated material does not have any pores shows that the level of atomic bonding between powder particles is substantially lower

than 100%. The decrease of the fracture strength of the forged discs with increasing  $\text{Al}_2\text{O}_3$  volume fraction shows that the level of interparticle atomic bonding decreases with increasing  $\text{Al}_2\text{O}_3$  volume fraction. As shown in Fig. 12c–e, the tensile testing specimens cut from the Cu–(5, 7.5, 10) vol% $\text{Al}_2\text{O}_3$  fractured at locations close to the locations of section width change. This shows that the cause of the specimen fracture is associated with stress concentration at the corners even though the corners are not sharp at all. This link in one way reflects the low tolerance of the consolidated material to stress concentration perhaps due to the lack of complete atomic bonding between the particles, and in another way also shows that the true strength of the interparticle bonds might be much higher than the measured fracture strength. To some extent, this complicates the correlation between the measured fracture strength of the consolidated material and other factors.

It is intriguing in trying to understand why with similar heating and forging conditions, the level of consolidation of the ultrafine-grained Cu powder and nanostructured Cu–2.5 vol% $\text{Al}_2\text{O}_3$  composite powder was high, while that of the other three Cu– $\text{Al}_2\text{O}_3$  composite powders was low. One of the reasons might be that the high relative densities of the Cu and Cu–2.5 vol% $\text{Al}_2\text{O}_3$  powder compacts strongly contribute to achieving the high level of consolidation through achieving a high level of sintering during the rapid induction heating. Another reason might be that the not-so-high relative densities of the Cu–(5, 7.5 and 10) vol% $\text{Al}_2\text{O}_3$  powder compacts (<80%) and the relatively high hot hardness of the powder particles with relatively high  $\text{Al}_2\text{O}_3$  fractions may allow extensive rearrangement and rotation of the powder particles to occur instead of particle deformation during forging. This may prevent formation of a large fraction of atomically fresh particle surfaces and rapid establishment of a high level of interparticle bonding, as discussed by Zhang et al. [1, 2]. Overall, it is important and would be rewarding to understand the mechanisms of rapidly establishing a high level of interparticle atomic bonding during thermomechanical powder consolidation of metallic and metal matrix composite powders and the key factors controlling the process. This systematic study provides some vital clues for this understanding, but further work is necessary to achieve a more in-depth understanding.

## Conclusions

A high level of consolidation of a ultrafine-grained Cu powder and a nanostructured Cu–2.5 vol% $\text{Al}_2\text{O}_3$  composite powder has been achieved by warm powder compacting at 300 °C followed by powder compact forging at 500 and 700 °C. However, this high level of powder consolidation

cannot be accomplished using the same process for nanostructured Cu–(5, 7.5 and 10) vol%Al<sub>2</sub>O<sub>3</sub> composite powders, possibly due to their higher powder particle hardness at elevated temperatures in the range of 300–800 °C. The microstructure of the ultrafine-grained Cu powder particles is refined during powder consolidation by warm powder compacting followed by powder compact forging, possibly due to recrystallization. In the meantime, the magnitude of Cu grain coarsening of the nanostructured Cu–(2.5–10) vol%Al<sub>2</sub>O<sub>3</sub> composite powder particles in the same powder consolidation process is small, possibly due to the high thermal stability of the microstructure caused by the pinning effect of Al<sub>2</sub>O<sub>3</sub> nanoparticles.

## References

- Zhang DL, Koch CC, Scattergood RO (2009) Mater Sci Eng A 516:270
- Zhang DL, Muhktar A, Nadakuduru VN, Raynova S (2009) Int J Mater Res (formerly Z Metallkd) 100:1720
- Haouaoui M, Karaman I, Maier HJ, Hartwig KT (2004) Met Mater Trans 35A:2935
- Karaman I, Haouaoui M, Maier HJ (2007) J Mater Sci 42:1561. doi:[10.1007/s10853-006-0987-6](https://doi.org/10.1007/s10853-006-0987-6)
- Xu W, Honma T, Wu X, Ringer SP, Xia K (2007) Appl Phys Lett 91:031901
- Lee Z, Zhou F, Valiev RZ, Lavernia EJ, Nutt SR (2004) Scr Mater 51:209
- Alexandrov IV, Zhu YT, Lowe TC, Islamgaliev RK, Valiev RZ (1998) NanoStruct Mater 10:45
- Stolyarov VV, Zhu YT, Lowe TC, Islamgaliev RK, Valiev RZ (2000) Mater Sci Eng A 282:78
- Yavari AR, Botta Filho WJ, Rodrigues CAD, Cardoso C, Valiev RZ (2002) Scr Mater 46:711
- Zhang DL, Raynova S, Nadakuduru V, Cao P, Gabbitas B, Robinson B (2009) Mater Sci Forum 618–619:513
- Shaik GR, Milligan WW (1997) Met Mater Trans A 28A:895
- Champion Y, Langlois C, Guérin-Mailly S, Langlois P, Bonnentien J, Hýtch M (2003) Science 300:310
- Correia JB, Marques MT, Oliveira MM, Matteazzi P (2001) Mater Sci Forum 360–362:241
- Witkin DB, Lavernia EJ (2006) Prog Mater Sci 51:1
- Botcharova E, Freudenberger J, Schultz L (2006) Acta Mater 54:3333
- He L, Allard LF, Breder K, Ma E (2000) J Mater Res 15:904
- Srivatsan TS, Ravi BG, Naruka AS, Petraroli M, Kalyanaraman R, Sudarshan TS (2002) Mater Des 23:291
- Molénat G, Thomas M, Galy J, Courret A (2007) Adv Eng Mater 9:667
- Um TY, Abe T, Sumi S (1999) J Mater Synth Process 7:303
- Mei BC, Miyamoto Y (2001) Metall Mater Trans 32A:843
- Youssif KM, Scattergood RO, Murty KL, Koch CC (2004) Appl Phys Lett 85:929
- Zhang DL, Raynova S, Koch CC, Scattergood RO, Youssif KM (2005) Mater Sci Eng A 410–411:375
- Youssif KM, Scattergood RO, Murty KL, Koch CC (2006) Scr Mater 54:251
- Cheng S, Ma E, Wang YM, Kecskes LJ, Youssif KM, Koch CC, Trociewitz UP, Han K (2005) Acta Mater 53:1521
- Zhang DL, Mukhtar A, Kong C, Munroe P (2009) J Phys: Conf Ser 144:012028
- Williamson GK, Hall W (1953) Acta Metall 2:22
- Mukhtar A, Zhang DL, Kong C, Munroe P (2009) J Phys: Conf Ser 144:012082